





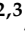
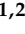





Article

Comparing the Performance of Supported Ru Nanocatalysts Prepared by Chemical Reduction of RuCl₃ and Thermal Decomposition of Ru₃(CO)₁₂ in the Sunlight-Powered Sabatier Reaction

Daria Burova ^{1,2,3} , Jelle Rohlfs ⁴ , Francesc Sastre ⁴ , Pau Martínez Molina ⁴ , Nicole Meulendijks ⁴ , Marcel A. Verheijen ^{5,6} , An-Sofie Kelchtermans ^{1,2,3} , Ken Elen ^{1,2,3} , An Hardy ^{1,2,3} , Marlies K. Van Bael ^{1,2,3,*} , and Pascal Buskens ^{1,4,*} 

- ¹ Institute for Materials Research, Design and Synthesis of Inorganic Materials (DESINE), Hasselt University, Agoralaan Building D, B-3590 Diepenbeek, Belgium; daria.burova@uhasselt.be (D.B.); ansofie.kelchtermans@uhasselt.be (A.-S.K.); ken.elen@uhasselt.be (K.E.); an.hardy@uhasselt.be (A.H.)
- ² IMEC VZW, IMOMEC Associated Laboratory, Wetenschapspark 1, B-3590 Diepenbeek, Belgium
- ³ EnergyVille, Thor Park 8320, B-3600 Genk, Belgium
- ⁴ The Netherlands Organisation for Applied Scientific Research (TNO), High Tech Campus 25, 5656AE Eindhoven, The Netherlands; jelle.rohlfstno.nl (J.R.); francesc.sastre@calbuig.tno.nl (F.S.); martinezmolina.pau@gmail.com (P.M.M.); nicole.meulendijks@tno.nl (N.M.)
- ⁵ Department of Applied Physics, Eindhoven University of Technology, 5600MB Eindhoven, The Netherlands; marcelverheijen@eurofinseag.com
- ⁶ Eurofins Materials Science, High Tech Campus 11, 5656AE Eindhoven, The Netherlands
- * Correspondence: marlies.vanbael@uhasselt.be (M.K.V.B.); pascal.buskens@tno.nl (P.B.)



Citation: Burova, D.; Rohlfs, J.; Sastre, F.; Molina, P.M.; Meulendijks, N.; Verheijen, M.A.; Kelchtermans, A.-S.; Elen, K.; Hardy, A.; Van Bael, M.K.; et al. Comparing the Performance of Supported Ru Nanocatalysts Prepared by Chemical Reduction of RuCl₃ and Thermal Decomposition of Ru₃(CO)₁₂ in the Sunlight-Powered Sabatier Reaction. *Catalysts* **2022**, *12*, 284. <https://doi.org/10.3390/catal12030284>

Academic Editors: Son Ich Ngo and Enrique García-Bordejé

Received: 30 January 2022

Accepted: 1 March 2022

Published: 2 March 2022

Publisher's Note: MDPI stays neutral with regard to jurisdictional claims in published maps and institutional affiliations.



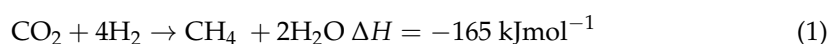
Copyright: © 2022 by the authors. Licensee MDPI, Basel, Switzerland. This article is an open access article distributed under the terms and conditions of the Creative Commons Attribution (CC BY) license (<https://creativecommons.org/licenses/by/4.0/>).

Abstract: The preparation of Ru nanoparticles supported on γ -Al₂O₃ followed by chemical reduction using RuCl₃ as a precursor is demonstrated, and their properties are compared to Ru nanoparticles supported on γ -Al₂O₃ prepared by impregnation of γ -Al₂O₃ with Ru₃(CO)₁₂ and subsequent thermal decomposition. The Ru nanoparticles resulting from chemical reduction of RuCl₃ are slightly larger (1.2 vs. 0.8 nm). In addition, Ru nanoparticles were deposited on Stöber SiO₂ using both deposition techniques. These particles were larger than the ones deposited on γ -Al₂O₃ (2.5 and 3.4 nm for chemical reduction and thermal decomposition, respectively). Taking into account the size differences between the Ru nanoparticles, all catalysts display similar activity (0.14–0.63 mol·g_{Ru}⁻¹·h⁻¹) and selectivity ($\geq 99\%$) in the sunlight-powered Sabatier reaction. Ergo, the use of toxic and volatile Ru₃(CO)₁₂ can be avoided, since catalysts prepared by chemical reduction of RuCl₃ display similar catalytic performance.

Keywords: carbon dioxide; methane; surface plasmon resonance; photocatalysis; photothermal

1. Introduction

As a society, we are currently facing two major challenges: reducing CO₂ emissions and the replacement of fossil fuels with green and sustainable energy sources and carriers. The sunlight-powered conversion of CO₂ to chemicals and fuels simultaneously addresses both challenges. CH₄ is an interesting energy carrier because of its high gravimetric storage density and everyday usage as a fuel. The Sabatier process is a well-known chemical reaction for the conversion of CO₂ and (green) H₂ to CH₄ in the presence of a supported metal catalyst (Equation (1)) [1].



The first and most popular catalyst for this reaction is Ni because of its low cost and wide abundance. Ni promotes CH₄ formation with a selectivity close to 100% [2–4]. These

and other supported metal catalysts for the Sabatier reaction, such as Ru and Rh, require thermal activation at temperatures between 300 and 500 °C [5]. Instead of conventional heating, sunlight is an appealing and green alternative in the case of photo(thermal) catalysis. Catalysts comprising metal nanoparticles with a plasmonic resonance in the UV-vis-NIR region are of interest for sunlight-powered reactions [6]. Based on their localized surface plasmon resonance (LSPR), light illumination induces a resonant response of free electrons in metallic nanoparticles [7,8]. This coherent oscillation dephases non-radiatively and generates hot electrons. These can influence reactions in two ways: they can be transferred to an electron-accepting orbital of an adsorbate in close proximity, or thermalize via electron–electron and electron–phonon scattering increasing the catalyst temperature. The LSPR of metallic nanoparticles can easily be tuned by varying the type of metal, size, shape and architecture of the particle, which makes this concept interesting for visible light and sunlight catalysis [9].

Typical catalysts reported for the (sun)light-powered Sabatier reaction are nanoparticles of group VIII metals supported on metal oxides [10,11]. Even though they do not demonstrate a strong LSPR in the visible light—their LSPR is weak and located in the UV region [12]—they display a strong photoabsorption ability [10]. Ru combines high activity with high selectivity towards CH₄ in the sunlight-powered conversion of CO₂ and H₂ [13,14]. Other examples of group VIII metals reported for this reaction are Au, Pd and Rh [15–17]. The most popular support materials are oxides, for example, Al₂O₃, SiO₂, TiO₂ and CeO_{2–x} [18–22]. They prevent the sintering of metal nanoparticles during their synthesis and use, and increase the dispersion and stability of the metal nanoparticle catalyst. The importance of the support material for the stability of the catalyst was demonstrated for Pt nanocatalysts on Al₂O₃, where weak electrostatic interaction between support and metal particles led to the formation of agglomerates and, as a consequence, to the loss of the catalytic activity [23]. Supported metal catalysts can be practically applied in different shapes, e.g., as powders and pellets [24,25]. Another key point is the influence of the support material on the reaction mechanism: for Rh and Ru supported on Al₂O₃, CO₂ adsorbs on the support, dissociates to CO and O, CO hydrogenates to CHO, then it dissociates to CH and O (rate-determining step, RDS), followed by fast hydrogenation of CH to produce CH₄ [26–28]. On the contrary, on oxide supports with oxygen vacancies such as CeO_{2–x}, Ce³⁺ acts as a Lewis base and initiates the formation of carboxylate CO₂^{δ–}, followed by hydrogenation to formate, which dissociates to form methanol, and, finally methanol is hydrogenated to CH₄, where the dissociation of formate to methanol is the RDS [29].

In addition to illuminated Ru nanoparticles serving as a nanosource of heat and/or electrons, Lee and coworkers proposed an alternative mechanism to explain the light-induced enhancement of the catalytic process, in which the energy gap of the CO₂ adsorbed on the metallic Ru surface plays a role in increasing the conversion rate and not only the light absorption of the metallic nanoparticle itself [30]. Lee and coworkers proposed that when CO₂ is adsorbed on the Ru (111) surface, its electronic structure changes: the energy gap decreases from 8.5 eV (for the free molecule) to 2.4 eV (CO₂ adsorbed on the Ru surface), and it increases the rate of CO₂ dissociation as the first step in the reaction mechanism.

In this manuscript, we focus on Ru nanoparticles supported on dielectric carrier materials, viz. γ -Al₂O₃ and Stöber SiO₂, as catalyst. We selected Ru nanoparticles based on their broadband light absorption, which makes them capable of harvesting a large part of the solar energy, their high catalytic activity and their ability to selectively convert CO₂ and H₂ to CH₄ [31]. Since the CH₄ production costs are dominated by the cost price of green H₂, there is currently no need to scout for low-cost alternatives to Ru [32]. We excluded semiconductive support materials such as TiO₂ and CeO_{2–x}, since they can generate electron-hole pairs using the UV part of sunlight and may directly catalyze the solar methanation reaction.

To validate whether collective effects such as plasmon coupling or collective photothermal heating play a role in the sunlight-powered Ru-catalyzed Sabatier reaction, Grote

et al. [33] studied spheroidal Ru-nanoparticles on γ -Al₂O₃ support, synthesized by impregnation of γ -Al₂O₃ with Ru₃(CO)₁₂ followed by high temperature annealing under N₂. They observed that the activity of the catalyst upon sunlight illumination increased superlinearly with a higher loading of metal in the catalyst. This effect was attributed to collective photothermal heating, which was further supported by continuous flow experiments [34] and multipoint temperature measurements inside the illuminated catalyst bed [35].

Since Ru₃(CO)₁₂ is a volatile chemical which is acutely toxic upon inhalation, we scouted a non-volatile precursor to prepare Ru nanospheres on metal oxide supports. For that purpose, we applied RuCl₃ using a deposition-precipitation sequence, followed by chemical reduction to obtain Ru nanoparticles similar to the ones obtained via thermal decomposition of Ru₃(CO)₁₂. Although the preparation of supported Ru catalysts using a deposition-precipitation sequence has been reported previously [18,36], the performance of catalysts produced in that manner has never been validated in comparison to Ru₃(CO)₁₂-derived catalysts for the sunlight-powered Sabatier reaction. The research question of the study at hand is whether the preparation technique affects the catalyst's chemical composition and nanostructure, and consequently the functional performance of the catalyst in the sunlight-powered Sabatier reaction. To address this question, we compare the catalytic performance of Ru nanoparticles prepared by impregnation and thermal decomposition of Ru₃(CO)₁₂ and deposition-precipitation and chemical reduction using RuCl₃ on two different dielectric metal oxide supports, viz. Stöber SiO₂ and γ -Al₂O₃. Availability of information on the relationship between the preparation technique, chemical composition and nanostructure, and functional performance facilitates the design and discovery of new nanocatalysts [37].

2. Results and Discussion

2.1. Synthesis and Characterization of Ru/SiO₂ and Ru/Al₂O₃ Catalysts

Two different methods were used for decoration of the supports, viz. γ -Al₂O₃ and Stöber SiO₂, with Ru nanoparticles: (1) deposition-precipitation followed by chemical reduction using RuCl₃ as a precursor (CR), and (2) impregnation with Ru₃(CO)₁₂ and subsequent high-temperature decomposition (TD). An overview of all catalysts prepared in this study is provided in Table 1. The composition and structure of these catalysts and their catalytic performance are compared to previous results obtained with Al₂O₃-TD catalysts [33].

Table 1. Catalysts prepared with different Ru loading (% *w/w*, obtained by ICP-EOS analyses) using Ru₃(CO)₁₂ and subsequent high-temperature decomposition (marked with TD) and deposition-precipitation followed by chemical reduction using RuCl₃ as a precursor (marked with CR).

Carrier Material	Loading, %			
SiO ₂ -TD	4.84	3.49	2.15	0.96
SiO ₂ -CR	3.88	3.34	2.05	0.98
Al ₂ O ₃ -CR	3.89	-	-	-

2.1.1. Deposition-Precipitation with Following Chemical Reduction (CR) Using RuCl₃

A slurry and dispersion of γ -Al₂O₃ and Stöber SiO₂, respectively, were prepared in aqueous urea. RuCl₃ and HCl were added to the mixture and then treated at 80 °C for 5 h to perform the deposition of Ru³⁺ and precipitation of ruthenium(III) oxide-hydroxide species on the surface of the support. Then, NaBH₄ was added to reduce the deposited ruthenium(III) oxide-hydroxide and form Ru nanoparticles. For Stöber SiO₂ as support, four different quantities of RuCl₃ were added to produce catalyst powders with theoretical Ru loadings of 1, 2.5, 4 and 6% *w/w*. For γ -Al₂O₃ as support, we aimed at preparing one catalyst with a theoretical Ru loading of 6% *w/w*. The resulting black catalyst materials were characterized using inductively coupled plasma optical emission spectrometry (ICP-OES, Table 1) to determine the Ru content and transmission electron microscopy (TEM,

Figure 1) to determine the size and shape of the Ru nanoparticles and their distribution over the SiO₂ and Al₂O₃ support surfaces.

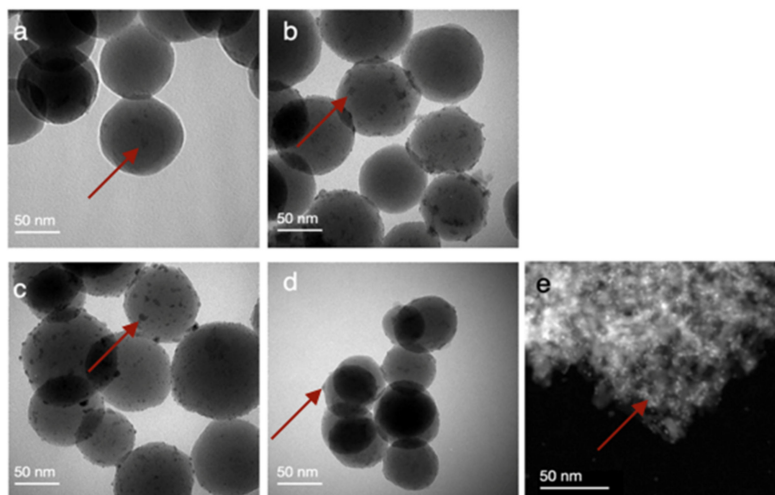


Figure 1. Bright-field TEM images of Ru nanoparticle catalysts on SiO₂ and γ -Al₂O₃ prepared by deposition-precipitation with following chemical reduction using RuCl₃, and with a Ru loading on silica of (a) 0.98% *w/w*, (b) 2.05% *w/w*, (c) 3.34% *w/w* and (d) 3.88% *w/w*, (e) and on alumina of 3.89% *w/w* (high-angle annular dark-field scanning transmission electron microscopy). The red arrows illustratively point out a supported Ru nanoparticle.

ICP-OES analyses performed on catalysts digested in a mixture of HCl, HNO₃ and HF yielded practically achieved Ru loadings of 0.98, 2.05, 3.34 and 3.88% *w/w* on Stöber SiO₂ (for 1, 2.5, 4 and 6% *w/w* theoretical loading) and 3.89% *w/w* (for 6% *w/w* theoretical loading) on γ -Al₂O₃. The TEM analyses demonstrate that small spheroidal Ru particles are randomly distributed over the surface of the Stöber SiO₂ (Figure 1a–d) and γ -Al₂O₃ (Figure 1e). The size of the Ru nanoparticles deposited on Stöber SiO₂ ($d = 50 \pm 5$ nm) was 2.5 ± 0.8 nm and remained constant with increasing Ru loading. Some agglomerates were observed, and their size did not exceed 8.9 nm. The size of the Ru nanoparticles deposited on γ -Al₂O₃ was 1.2 ± 0.5 nm and no agglomerates were observed. This is larger than the size previously reported for Ru nanoparticles on γ -Al₂O₃ obtained via thermal decomposition (0.8 nm) [33]. In previous work, we have confirmed that Ru nanoparticles obtained via thermal decomposition of Ru₃(CO)₁₂ are metallic in nature, and excluded the presence of RuO₂ [33]. To confirm this for the catalysts prepared via chemical reduction of RuCl₃, we performed XRD analysis. Due to the low loading and small particle size, however, Ru reflections could not be detected (Figure S1). Furthermore, we performed thermogravimetric analyses (TGA) in air to evaluate if we could detect a mass increase in the sample because of the oxidation of Ru to RuO₂ at elevated temperatures (Figure S2). A mass decrease of about 10% due to the loss of adsorbed water and progressive condensation of Si–OH and Al–OH groups made it impossible to detect a potential small increase (<1% expected) due to the oxidation of Ru. Since we observe no increase in the reaction rate over time (see Section 2.2.), which we previously observed when using supported RuO₂ catalysts that reduced to metallic Ru during the first minutes of the reaction [14], we assume that our catalysts comprise metallic Ru.

2.1.2. Impregnation with Ru₃(CO)₁₂ and Subsequent Thermal Decomposition (TD)

For the second method, the procedure reported by Grote et al. [33] was used: the impregnation of Stöber SiO₂ with Ru₃(CO)₁₂ as ruthenium precursor followed by high-temperature treatment in an inert atmosphere. The loading of Ru was controlled by the ratio of Ru₃(CO)₁₂ to support material. ICP-OES analyses showed Ru loadings of 0.96, 2.15, 3.49 and 4.84% *w/w* on Stöber SiO₂, when aiming for theoretical loadings of 1, 2.5, 4

and 6% *w/w* (Table 1). TEM analyses demonstrated a homogeneous dispersion of small spheroidal ruthenium nanoparticles of larger size than the ones obtained using RuCl_3 for all Ru loadings (3.4 ± 1.2 vs. 2.5 ± 0.8 nm, Figure 2).

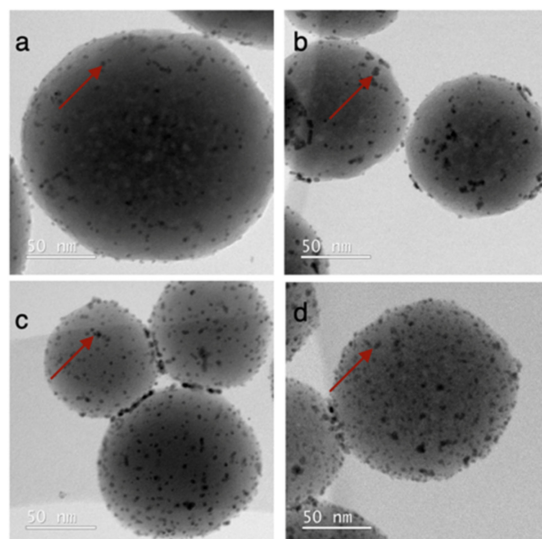


Figure 2. TEM analyses of Ru nanoparticle catalysts on SiO_2 , prepared by impregnation with $\text{Ru}_3(\text{CO})_{12}$ and subsequent thermal decomposition, and with a Ru loading of (a) 0.96% *w/w*, (b) 2.15% *w/w*, (c) 3.49% *w/w* and (d) 4.84% *w/w*. The red arrows illustratively point out a supported Ru nanoparticle.

2.2. Catalyst Performance in the Sunlight-Powered Sabatier Reaction

Our previous work demonstrated that Ru nanoparticles supported on $\gamma\text{-Al}_2\text{O}_3$, prepared via impregnation with $\text{Ru}_3(\text{CO})_{12}$ and subsequent thermal decomposition, are efficient catalysts for the sunlight-powered Sabatier reaction [33]. To investigate whether the way of production affects the catalytic performance, comparative experiments with $\text{Ru}/\text{Al}_2\text{O}_3$ produced via deposition-precipitation followed by chemical reduction using RuCl_3 were carried out ($\text{Ru}/\text{Al}_2\text{O}_3\text{-CR}$, 3.89% *w/w*). To determine the activity of the catalyst in the sunlight-powered Sabatier process, $\text{Ru}/\text{Al}_2\text{O}_3\text{-CR}$ was tested at a catalyst bed temperature of approximately 220 °C, realized via combined heating of the reactor to a starting temperature of 150 °C and illumination. In the latter case, a solar simulator illuminated the catalyst bed with a light intensity of 6.6 suns resulting in a catalyst bed temperature of approximately 220 °C. Under these conditions, CH_4 was produced as the sole reaction product at a starting rate of $0.46 \text{ mol}\cdot\text{g}_{\text{Ru}}^{-1}\cdot\text{h}^{-1}$ (Figure 3).

This value is slightly lower than the previously reported activity for $\text{Ru}/\text{Al}_2\text{O}_3$ produced via impregnation with $\text{Ru}_3(\text{CO})_{12}$ and subsequent thermal decomposition (TD, $0.63 \text{ mol}\cdot\text{g}_{\text{Ru}}^{-1}\cdot\text{h}^{-1}$, Figure 3). For the dark reaction with both catalysts at 220 °C, we observed a reaction rate of $0.49 \text{ mol}\cdot\text{g}_{\text{Ru}}^{-1}\cdot\text{h}^{-1}$ (CR) and $0.29 \text{ mol}\cdot\text{g}_{\text{Ru}}^{-1}\cdot\text{h}^{-1}$ (TD, Figure 3).

Overall, the catalytic activity and selectivity of $\text{Ru}/\text{Al}_2\text{O}_3\text{-TD}$ and $\text{Ru}/\text{Al}_2\text{O}_3\text{-CR}$ are within the same order of magnitude. Potential reasons for the observed minor differences in activity between catalysts prepared with different Ru deposition techniques may be the presence of remaining species that block catalytic sites in the catalyst produced via chemical reduction, and the larger particle size of the Ru nanoparticles obtained from RuCl_3 (1.2 vs. 0.8 nm [33]). Based on the catalytic performance of the $\text{Ru}/\text{Al}_2\text{O}_3$ catalyst, we conclude that the deposition-precipitation followed by the chemical reduction is a suitable alternative method for producing Ru nanocatalysts. The result of the catalytic experiments demonstrates that the use of volatile and toxic $\text{Ru}_3(\text{CO})_{12}$ can be avoided. Besides the preparation method, two carrier materials—Stöber SiO_2 and $\gamma\text{-Al}_2\text{O}_3$ —were compared under identical reaction conditions using both preparation methods. Samples with similar Ru loading were taken for comparison (between 3.49% *w/w* and 3.89% *w/w*

Ru). The conversion-time profile for Ru/SiO₂ obtained by the deposition-precipitation with chemical reduction almost coincides with that of Ru/Al₂O₃ obtained by the same method, reflected by their initial reaction rates of 0.37 mol·g_{Ru}⁻¹·h⁻¹ for Ru/SiO₂-CR vs. 0.46 mol·g_{Ru}⁻¹·h⁻¹ for Ru/Al₂O₃-CR (Figure 4). In the absence of H₂, Ru catalysts prepared by chemical reduction of RuCl₃ do not promote conversion of CO₂ to CH₄ or other products. In previous work, we have also demonstrated this for Ru catalysts prepared via thermal decomposition of Ru₃(CO)₁₂ [33].

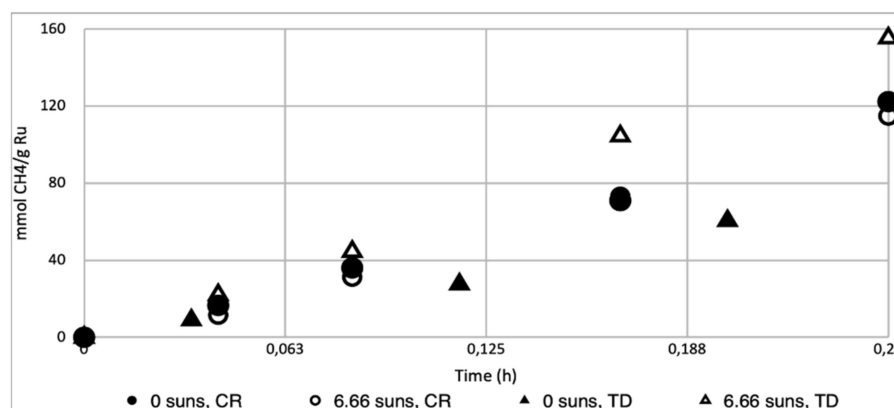


Figure 3. Conversion-time profile for the Sabatier reaction carried out in dark (0 suns) and light conditions (6.66 suns) with Ru/Al₂O₃ catalysts prepared using Ru₃(CO)₁₂ (TD, 3.6% w/w Ru) [33] and RuCl₃ (CR, 3.89% w/w). Reaction conditions for all experiments: reaction mixture of H₂/CO₂/N₂ (4.5:1:1) at 3.5 ± 0.2 bar pressure, 200 mg of Ru/Al₂O₃ or Ru/SiO₂ catalyst, catalyst bed temperature of approximately 220 °C.

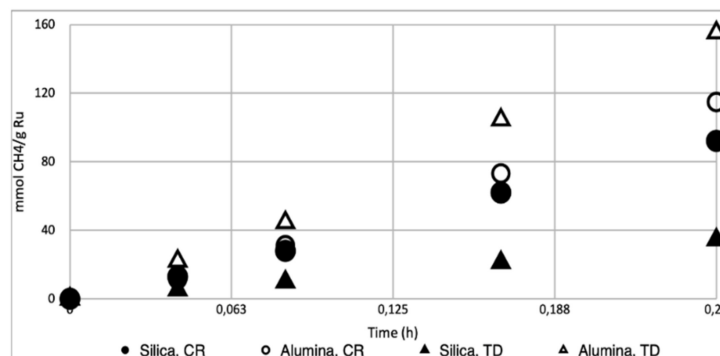


Figure 4. Conversion-time profile for the Sabatier reaction carried out in light conditions (6.66 suns) with Ru/Al₂O₃ catalysts prepared using Ru₃(CO)₁₂ (TD, 3.6% w/w Ru, Δ) [33] and RuCl₃ (CR, 3.89% w/w, ○), and their SiO₂ supported counterparts Ru/SiO₂-TD (3.49% w/w, ▲) and Ru/SiO₂-CR (3.88% w/w, ●). Reaction conditions for all experiments: reaction mixture of H₂/CO₂/N₂ (4.5:1:1) at 3.5 ± 0.2 bar pressure, 200 mg of Ru/Al₂O₃ or Ru/SiO₂ catalyst, catalyst bed temperature of approximately 220 °C.

However, for the catalysts obtained using thermal decomposition of Ru₃(CO)₁₂, the slope of the Ru/SiO₂-TD curve showed a lower initial rate than Ru/Al₂O₃-TD [33] (0.14 vs. 0.63 mol·g_{Ru}⁻¹·h⁻¹). This is caused by the substantial difference in Ru particle size for catalysts and related surface area obtained using both preparation techniques: 3.4 nm for Ru/SiO₂-TD vs. 0.8 nm for Ru/Al₂O₃-TD.

To validate their potential for reuse, we evaluated the catalytic performance of Ru/SiO₂-TD and Ru/SiO₂-CR with Ru loadings of 3.49% w/w and 3.34% w/w, respectively, in three sequential reaction runs. In all of these experiments, we combined sunlight illumination (6.66 suns) with conventional heating of the reactor to achieve a catalyst bed temperature

of 220 °C. For the experiments performed with Ru/SiO₂-TD, we observed a similar reaction rate in all three runs (0.14 mol·g_{Ru}⁻¹·h⁻¹ in run 1, 0.15 mol·g_{Ru}⁻¹·h⁻¹ in run 2 and 0.14 mol·g_{Ru}⁻¹·h⁻¹ in run 3) (Figure S3). For the experiments performed with Ru/SiO₂-CR, we observed a decrease in reaction rate from run 1 to run 3 of 28% (0.37 mol·g_{Ru}⁻¹·h⁻¹ in run 1, 0.35 mol·g_{Ru}⁻¹·h⁻¹ in run 2 and 0.27 mol·g_{Ru}⁻¹·h⁻¹ in run 3). This may be explained by progressive agglomeration of Ru on the SiO₂ surface during the catalytic reactions, as illustrated by bright-field (BF) TEM analyses of the same catalyst before run 1 and after run 3 (Figure 5). The degree of agglomeration is 52%, and typical agglomerate sizes are 9.5 nm (Figure S4).

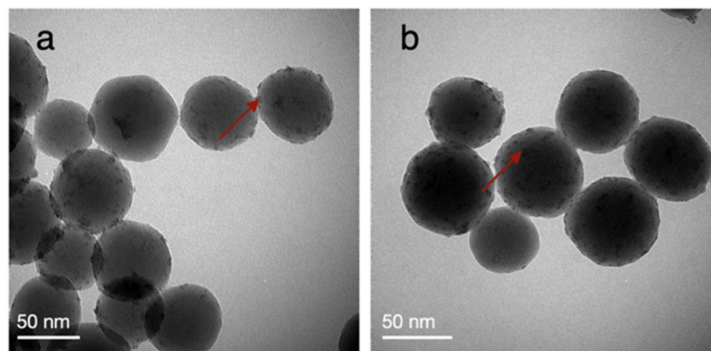


Figure 5. BFTEM images of Ru/SiO₂-CR with a Ru loading of 3.34% *w/w* (a) before and (b) after sunlight-powered Sabatier's reaction. Reaction conditions: reaction mixture of H₂/CO₂/N₂ (4.5:1:1) at 3.5 ± 0.2 bar pressure, 200 mg of Ru/Al₂O₃ or Ru/SiO₂ catalyst, light intensity of 6.66 suns, catalyst bed temperature of approximately 220 °C. The red arrows illustratively point out a supported Ru nanoparticle.

3. Materials and Methods

3.1. Catalyst Synthesis

3.1.1. Synthesis of Stöber SiO₂ Support

SiO₂ nanoparticles were prepared according to the Stöber process by hydrolysis and condensation of tetraethyl orthosilicate (TEOS) [38]. For the preparation of 50 nm sized SiO₂ particles, ethanol (40 mL, VWR Chemicals, Radnor, PA, USA, 98%), H₂O (1 mL, milliQ grade), and aqueous ammonia (3 mL, VWR Chemicals, Radnor, PA, USA, 32% in water) were mixed in a 250 mL flask and stirred for 5 min. Then, TEOS (4 mL) dissolved in EtOH (30 mL) was added. The mixture was stirred at 25 °C for 5 h. The obtained SiO₂ nanoparticles were washed twice with water (milliQ grade) after 10 min centrifugation (11,000 × *g* rpm) and dried at 100 °C for 2 h.

3.1.2. Synthesis of Ru/SiO₂ Catalyst: Deposition-Precipitation with Following Chemical Reduction Using RuCl₃

For the synthesis of Ru/SiO₂ with a theoretical Ru loading of 2.5 *w/w*%, Stöber SiO₂ nanoparticles (400 mg) were dispersed in an aqueous urea solution (20 mL, 2.5 M in milliQ water, ACROS Organics, Geel, Belgium, 99%), after which an aqueous solution of ruthenium (III) chloride hydrate (0.02 M in 0.1 M HCl; Aldrich, St. Louis, MO, USA, 40–49% ruthenium; HCl, VWR Chemicals, Radnor, PA, USA, 37% in water; 5 mL) was added and ultrasonicated for 10 min. Next, the resulting mixture was heated for 5 h at 80 °C. After that, NaBH₄ solution (0.01 M in milliQ water; 5 mL) was added and the reaction mixture was further heated for 30 min. Finally, the Ru/SiO₂ catalyst particles were filtered and washed three times with water and once with ethanol. The catalyst was dried at room temperature for 24 h and stored in ambient conditions.

3.1.3. Synthesis Ru/SiO₂ Catalyst: Impregnation with Ru₃(CO)₁₂ and Subsequent Thermal Decomposition

This synthesis was performed in analogy to the protocol reported by Grote et al. for Ru/ γ -Al₂O₃ [33]: Ru₃(CO)₁₂ (ACROS Organics, Geel, Belgium, 99%) was dissolved in tetrahydrofuran (THF, VWR Chemicals, Radnor, PA, USA, GPR RECTAPUR grade, 99%) by stirring at room temperature for 30 min. After the silica nanoparticles were added to the solution, the resulting mixture was stirred for 2 h at room temperature, whereafter the THF was removed by rotary evaporation under reduced pressure at 80 °C. The precursor was decomposed under a N₂ inert gas atmosphere with a heating ramp of 5 °C·min⁻¹ until 300 °C and kept at 300 °C for 2 h, cooled down to room temperature and stored in ambient conditions.

3.1.4. Synthesis of Ru/Al₂O₃ Catalyst: Deposition-Precipitation with Following Chemical Reduction Using RuCl₃

γ -Al₂O₃ (Alfa Aesar, Haverhill, MA, USA, 99.97%, surface area 200 m²·g⁻¹) was calcined in air at 500 °C for 6 h. After cooling down to room temperature, the same procedure was carried out as for Ru/SiO₂ (procedure 2).

3.2. Characterization of the Catalyst

3.2.1. Dynamic Light Scattering

The particle size of Stöber SiO₂ and its distribution were characterized via dynamic light scattering (DLS), using a Brookhaven ZetaPals machine (Brookhaven Instruments Corporation, Holtsville, NY, USA). The Stöber SiO₂ particles were dispersed in milliQ water at pH = 7.5, and then measured in dispersion.

3.2.2. Electron Microscopy

The particle size and morphology of Ru/Al₂O₃ and Ru/SiO₂ catalysts were investigated using an FEI Tecnai Spirit Twin electron microscope (Thermo Fischer Scientific, Hillsboro, OR, USA). Imaging was performed in bright-field transmission electron microscopy (TEM) and high-angle annular dark field (HAADF) scanning transmission electron microscopy (STEM) mode. Samples for (S)TEM investigation were prepared by mixing the catalyst powder with ethanol, followed by deposition of the resulting suspension onto a Cu-supported holey carbon grid. Using the FEI Tecnai Spirit Twin electron microscope equipped with a Si (Li) Ametek EDX detector for energy-dispersive X-ray analysis, the Ru loading was analyzed. The number of Ru particle agglomerates was counted by analysis of all STEM pictures of each sample, listing and then determining the number of agglomerates by counting the particles with the diameter larger than the mean diameter of single Ru nanoparticle on the image. STEM-EDX mappings were acquired using a probe-corrected JEOL ARM 200F (Peabody, MA, USA), equipped with a 100 mm² SDD Centurio EDX detector.

3.2.3. Inductively Coupled Plasma Optical Emission Spectrometry

The Ru content of the catalysts was determined by inductively coupled plasma optical emission spectrometry (ICP-OES, Perkin Elmer Optima 3300 dv simultaneous spectrometer, PerkinElmer, Waltham, MA, USA). For Ru content analysis, catalyst (20 mg) was added to a teflon vessel with HCl (6 mL, VWR Chemicals, Radnor, PA, USA, 37%), HNO₃ (1 mL, VWR Chemicals, Radnor, PA, USA, 69%) and HF (3 mL, VWR Chemicals, Radnor, PA, USA, 40%). Microwave digestion was carried out in an Ethos UP reactor. After cooling down, the elemental analysis was carried out using an external calibration method (Ruthenium, AAS standard solution, Specpure, Ru 1000 µg/mL). All ICP analyses were carried out in duplo. The measurement error was evaluated based on calibration certificates and from statistical analysis of repeated measurements. The following errors were taken into account: the error of volumetric operations (pipettes, volumetric flasks, measuring cylinders), the error of balances and the error of concentrations/purity of commercial chemicals. For calculations,

calibration certificates or information sheets from the manufacturer were used. The main contributors were the error of calibration reference materials (1%) and the error of delivered volumes/masses. The absolute error did not exceed 1%.

3.3. Catalysis Experiments

For the photomethanation experiments, a custom-built photoreactor equipped with a solar simulator (Newport Sol3A, Newport Corporation, Irvine, CA, USA) and reaction cell with quartz window was used, as reported previously [33]. The mass of catalyst powder for one experiment was 200 mg. Every experiment was carried out according to the following procedure: the sample of catalyst powder on a quartz filter membrane was placed inside the reactor cell, after which the cap was closed tightly. Then, the temperature was stabilized at the desirable point with the internal heater. After temperature stabilization, the reactor was filled with the reaction mixture in the ratio $\text{H}_2:\text{N}_2:\text{CO}_2$ (4.5:1:1). The total pressure before the experiment was 3.5 ± 0.2 bars. During the experiments with non-zero light intensity, the sample was irradiated with a solar light simulator (provided with a filter of air mass coefficient 1.5 (AM 1.5)) from the top through the quartz window ($1 \text{ sun} = 0.1 \text{ W}\cdot\text{cm}^{-2}$). Once the light source was switched on, gas samples (5 to 7 mL) were taken every 2.5 or 5 min from the upper part of the reactor using a gas-tight syringe and directly analyzed by gas chromatography (compact GC Interscience, Interscience, Breda, The Netherlands). GC is equipped with three channels, two micro TCD detectors and one FID detector. The first channel used to measure H_2 , O_2 , N_2 and CO has a MolSieve 5 Å column and RT-Q bond precolumn and TCD detector. The second channel, used to measure H_2O and CO_2 , has a combination of the TR-U bond column and RT-Q bond column and TCD detector. The third channel, used to measure methane, ethane and propane, is fitted with a Rtx-1, 2u column and FID detector. The standard deviation for every measurement was based on the error of balance, equipment (gas chromatography machine, pressure sensor, temperature sensor, light source), and measuring tools such as syringes. The absolute error did not exceed 2%. For calibration curves for the GC quantification and a representative gas chromatogram, see Figures S5 and S6.

4. Conclusions

We successfully prepared small spheroidal Ru nanoparticles on the surface of Stöber SiO_2 and $\gamma\text{-Al}_2\text{O}_3$ using two different preparation techniques: impregnation of the metal oxide with $\text{Ru}_3(\text{CO})_{12}$ and subsequent thermal decomposition under N_2 inert gas atmosphere, and deposition-precipitation followed by chemical reduction using RuCl_3 as Ru precursor. Taking into account the difference in particle size of Ru obtained using both preparation techniques on $\gamma\text{-Al}_2\text{O}_3$ (0.8–1.2 nm) and Stöber SiO_2 (2.5–3.4 nm), the activity ($0.14\text{--}0.63 \text{ mol}\cdot\text{g}_{\text{Ru}}^{-1}\cdot\text{h}^{-1}$) and selectivity ($\geq 99\%$) of the catalysts for the sunlight-powered Sabatier process were similar. Ergo, the use of toxic and volatile $\text{Ru}_3(\text{CO})_{12}$ can be avoided, since catalysts prepared by chemical reduction of RuCl_3 display similar catalytic performance. However, the potential for reuse of Ru/ SiO_2 was better for catalysts obtained using $\text{Ru}_3(\text{CO})_{12}$ as precursor. Catalysts prepared using RuCl_3 suffered from progressive agglomeration of Ru nanoparticles on the SiO_2 surface, resulting in a decrease in reaction rate of 28% between the first and the third run. Future work in our group will focus on improving the stability of Ru catalysts prepared by deposition-precipitation followed by chemical reduction using RuCl_3 as Ru precursor to improve their potential for reuse.

Supplementary Materials: The following supporting information can be downloaded at: <https://www.mdpi.com/article/10.3390/catal12030284/s1>, Figure S1: X-ray diffractogram of SiO_2 supported Ru catalyst prepared by reduction of RuCl_3 , Figure S2: Thermogravimetric analyses of (a) SiO_2 -supported and (b) Al_2O_3 -supported Ru catalyst prepared by reduction of RuCl_3 , under air, Figure S3: Conversion-time profile for three sequential runs of the sunlight-powered Sabatier reaction with Ru/ SiO_2 -TD, Figure S4: Comparison of mean diameter of Ru nanoparticles and numbers of agglomerates before (a) and after (b) reaction for Ru/ SiO_2 -CR catalysts with a Ru loading on silica of 3.34% w/w, Figure S5: Calibration curves for GC detection of (a) H_2 , (b) N_2 , (c) CO_2 and (d) CH_4 ,

Figure S6: Prototypical gas chromatogram for catalytic conversion of CO₂ and H₂ to CH₄ in a mixture diluted with N₂.

Author Contributions: Conceptualization, M.K.V.B., P.B., A.H. and K.E.; methodology, D.B., J.R., F.S., P.B. and P.M.M.; validation, D.B., J.R. and P.M.M.; formal analysis, D.B. and P.B.; investigation, D.B., F.S. and P.M.M.; characterization, D.B., K.E., M.A.V. and A.-S.K.; writing—original draft preparation, D.B.; writing—review and editing, P.B., F.S., M.K.V.B., A.H., K.E. and N.M.; supervision, P.B., K.E., A.H. and M.K.V.B.; project administration, K.E. and N.M.; funding acquisition, P.B. and N.M. All authors have read and agreed to the published version of the manuscript.

Funding: This research was funded by the European Commission (H2020 project SPOTLIGHT, grant no. 722788).

Acknowledgments: M.A.V. acknowledges Solliance and the Dutch province of Noord-Brabant for funding the TEM facility. We acknowledge Ulrique Vounckx for performing TEM analyses.

Conflicts of Interest: The authors declare no conflict of interest.

References

1. Sabatier, P.; Senderens, J.B. New Synthesis of Methane. In *Comptes Rendus Hebdomadaires des Seances de l'Academie des Sciences; Biodiversity Heritage Library: Washington, DC, USA, 1902; Volume 134, pp. 514–516.*
2. Martínez, J.; Hernández, E.; Alfaro, S.; Medina, R.L.; Aguilar, G.V.; Albitzer, E.; Valenzuela, M.A. High Selectivity and Stability of Nickel Catalysts for CO₂ Methanation: Support Effects. *Catalysts* **2019**, *9*, 24. [[CrossRef](#)]
3. Vogt, C.; Monai, M.; Kramer, G.J.; Weckhuysen, B.M. The renaissance of the Sabatier reaction and its applications on Earth and in space. *Nat. Catal.* **2019**, *2*, 188–197. [[CrossRef](#)]
4. Rönsch, S.; Schneider, J.; Matthischke, S.; Schlüter, M.; Götz, M.; Lefebvre, J.; Prabhakaran, P.; Bajohr, S. Review on methanation—From fundamentals to current projects. *Fuel* **2016**, *166*, 276–296. [[CrossRef](#)]
5. Sabatier, P.; Senderens, J.-B. Direct Hydrogenation of Oxides of Carbon in Presence of Various Finely Divided Metals. *CR Acad. Sci.* **1903**, *134*, 689–691.
6. Mendonça, C.D.; Khan, S.U.; Rahemi, V.; Verbruggen, S.W.; Machado, S.A.S.; De Wael, K. Surface plasmon resonance-induced visible light photocatalytic TiO₂ modified with AuNPs for the quantification of hydroquinone. *Electrochim. Acta* **2021**, *389*, 138734. [[CrossRef](#)]
7. Sarhan, R.M.; Koopman, W.; Pudell, J.; Stete, F.; Rössle, M.; Herzog, M.; Schmitt, C.N.Z.; Liebig, F.; Koetz, J.; Bargheer, M. Scaling Up Nanoplasmon Catalysis: The Role of Heat Dissipation. *J. Phys. Chem. C* **2019**, *123*, 9352–9357. [[CrossRef](#)]
8. Cortés, E.; Besteiro, L.V.; Alabastri, A.; Baldi, A.; Tagliabue, G.; Demetriadou, A.; Narang, P. Challenges in Plasmonic Catalysis. *ACS Nano* **2020**, *14*, 16202–16219. [[CrossRef](#)]
9. Murray, W.; Barnes, W. Plasmonic materials. *Adv. Mater.* **2007**, *19*, 3771–3782. [[CrossRef](#)]
10. Meng, X.; Wang, T.; Liu, L.; Ouyang, S.; Li, P.; Hu, H.; Kako, T.; Iwai, H.; Tanaka, A.; Ye, J. Photothermal Conversion of CO₂ into CH₄ with H₂ over Group VIII Nanocatalysts: An Alternative Approach for Solar Fuel Production. *Angew. Chem. Int. Ed.* **2014**, *53*, 11478–11482. [[CrossRef](#)]
11. Reddy, N.L.; Rao, V.N.; Vijayakumar, M.; Santhosh, R.; Anandan, S.; Karthik, M.; Shankar, M.V.; Reddy, K.R.; Shetti, N.P.; Nadagouda, M.N.; et al. A review on frontiers in plasmonic nano-photocatalysts for hydrogen production. *Int. J. Hydrogen Energy* **2019**, *44*, 10453–10472. [[CrossRef](#)]
12. Sanz, J.M.; Ortiz, D.; Alcaraz de la Osa, R.; Saiz, J.M.; González, F.; Brown, A.S.; Losurdo, M.; Everitt, H.O.; Moreno, F. UV Plasmonic Behavior of Various Metal Nanoparticles in the Near- and Far-Field Regimes: Geometry and Substrate Effects. *J. Phys. Chem. C* **2013**, *117*, 19606–19615. [[CrossRef](#)]
13. Lunde, P.J.; Kester, F.L. Carbon Dioxide Methanation on a Ruthenium Catalyst. *Ind. Eng. Chem. Process Des. Dev.* **1974**, *13*, 27–33. [[CrossRef](#)]
14. Sastre, F.; Versluis, C.; Meulendijks, N.; Rodríguez-Fernández, J.; Sweelssen, J.; Elen, K.; Van Bael, M.K.; den Hartog, T.; Verheijen, M.A.; Buskens, P. Sunlight-Fueled, Low-Temperature Ru-Catalyzed Conversion of CO₂ and H₂ to CH₄ with a High Photon-to-Methane Efficiency. *ACS Omega* **2019**, *4*, 7369–7377. [[CrossRef](#)]
15. Aziz, M.A.A.; Jalil, A.A.; Triwahyono, S.; Ahmad, A. CO₂ methanation over heterogeneous catalysts: Recent progress and future prospects. *Green Chem.* **2015**, *17*, 2647–2663. [[CrossRef](#)]
16. Veith, G.M.; Lupini, A.R.; Rashkeev, S.; Pennycook, S.J.; Mullins, D.R.; Schwartz, V.; Bridges, C.A.; Dudney, N.J. Thermal stability and catalytic activity of gold nanoparticles supported on silica. *J. Catal.* **2009**, *262*, 92–101. [[CrossRef](#)]
17. Martin, N.M.; Hemmingsson, F.; Wang, X.; Merte, L.R.; Hejral, U.; Gustafson, J.; Skoglundh, M.; Meira, D.M.; Dippel, A.; Gutowski, O.; et al. Structure-function Relationship during CO₂ Methanation over Rh/Al₂O₃ and Rh/SiO₂ Catalysts at Atmospheric Pressure Conditions. *Catal. Sci. Technol.* **2018**, *8*, 2686–2696. [[CrossRef](#)]
18. Chai, S.; Men, Y.; Wang, J.; Liu, S.; Song, Q.; An, W.; Kolb, G. Boosting CO₂ methanation activity on Ru/TiO₂ catalysts by exposing (001) facets of anatase TiO₂. *J. CO₂ Util.* **2019**, *33*, 242–252. [[CrossRef](#)]

19. Lin, Q.; Liu, X.Y.; Jiang, Y.; Wang, Y.; Huang, Y.; Zhang, T. Crystal phase effects on the structure and performance of ruthenium nanoparticles for CO₂ hydrogenation. *Catal. Sci. Technol.* **2014**, *4*, 2058–2063. [[CrossRef](#)]
20. Garbarino, G.; Bellotti, D.; Finocchio, E.; Magistri, L.; Busca, G. Methanation of carbon dioxide on Ru/Al₂O₃: Catalytic activity and infrared study. *Catal. Today* **2016**, *277*, 21–28. [[CrossRef](#)]
21. Tada, S.; Shimizu, T.; Kameyama, H.; Haneda, T.; Kikuchi, R. Ni/CeO₂ catalysts with high CO₂ methanation activity and high CH₄ selectivity at low temperatures. *Int. J. Hydrogen Energy* **2012**, *37*, 5527–5531. [[CrossRef](#)]
22. Ashok, J.; Ang, M.L.; Kawi, S. Enhanced activity of CO₂ methanation over Ni/CeO₂-ZrO₂ catalysts: Influence of preparation methods. *Catal. Today* **2017**, *281*, 304–311. [[CrossRef](#)]
23. Parapat, R.Y.; Saputra, O.H.I.; Ang, A.P.; Schwarze, M.; Schomacker, R. Hot Electron and Surface Plasmon-Driven Catalytic Reaction in Metal–Semiconductor Nanostructures. *RSC Adv.* **2014**, *4*, 50955. [[CrossRef](#)]
24. Murena, F.; Esposito, S.; Deorsola, F.A.; Galletti, C.; Prati, M.V. CO₂ abatement and CH₄ recovery at vehicle exhausts: Comparison and characterization of Ru powder and pellet catalysts. *Int. J. Hydrogen Energy* **2020**, *45*, 8640–8648. [[CrossRef](#)]
25. Porta, A.; Falbo, L.; Visconti, C.G.; Lietti, L.; Bassano, C.; Deiana, P. Synthesis of Ru-based catalysts for CO₂ methanation and experimental assessment of intraporous transport limitations. *Catal. Today* **2020**, *343*, 38–47. [[CrossRef](#)]
26. Zhang, X.; Li, X.; Reish, M.E.; Zhang, D.; Su, N.Q.; Gutiérrez, Y.; Moreno, F.; Yang, W.; Everitt, H.O.; Liu, J. Plasmon-Enhanced Catalysis: Distinguishing Thermal and Nonthermal Effects. *Nano Lett.* **2018**, *18*, 1714–1723. [[CrossRef](#)] [[PubMed](#)]
27. Karelovic, A.; Ruiz, P. CO₂ hydrogenation at low temperature over Rh/-Al₂O₃ catalysts: Effect of the metal particle size on catalytic performances and reaction mechanism. *Appl. Catal. B Environ.* **2012**, *113–114*, 237–249. [[CrossRef](#)]
28. Avanesian, T.; Gusmão, G.S.; Christopher, P. Mechanism of CO₂ reduction by H₂ on Ru(0 0 1) and general selectivity descriptors for late-transition metal catalysts. *J. Catal.* **2016**, *343*, 86–96. [[CrossRef](#)]
29. Wang, F.; He, S.; Chen, H.; Wang, B.; Zheng, L.; Wei, M.; Evans, D.G.; Duan, X. Active Site Dependent Reaction Mechanism over Ru/CeO₂ Catalyst toward CO₂ Methanation. *J. Am. Chem. Soc.* **2016**, *138*, 6298–6305. [[CrossRef](#)]
30. Kim, C.; Hyeon, S.; Lee, J. Energy-efficient CO₂ hydrogenation with fast response using photoexcitation of CO₂ adsorbed on metal catalysts. *Nat. Commun.* **2018**, *9*, 3027. [[CrossRef](#)]
31. Kowalczyka, Z.; Stołecik, K.; Rarog-Pilecka, W.; Miskiewicz, E.; Wilczkowska, E.; Karpinski, Z. Supported ruthenium catalysts for selective methanation of carbon oxides at very low CO_x/H₂ ratios. *Appl. Catal. A Gen.* **2008**, *342*, 35–39. [[CrossRef](#)]
32. Van der Zwaan, B.; Detz, R.; Meulendijks, N.; Buskens, P. Renewable natural gas as climate-neutral energy carrier? *Fuel* **2022**, *311*, 122547. [[CrossRef](#)]
33. Grote, R.; Habets, R.; Rohlfs, J.; Sastre, F.; Meulendijks, N.; Xu, M.; Verheijen, M.A.; Elen, K.; Hardy, A.; Van Bael, M.K.; et al. Collective photothermal effect of Al₂O₃-supported spheroidal plasmonic Ru nanoparticle catalysts in the sunlight-powered Sabatier reaction. *ChemCatChem* **2020**, *12*, 5618–5622. [[CrossRef](#)]
34. Rohlfs, J.; Bossers, K.W.; Meulendijks, N.; Valega Mackenzie, F.; Xu, M.; Verheijen, M.A.; Buskens, P.; Sastre, F. Continuous-Flow Sunlight-Powered CO₂ Methanation Catalyzed by γ-Al₂O₃-Supported Plasmonic Ru Nanorods. *Catalysts* **2022**, *12*, 126. [[CrossRef](#)]
35. Xu, M.; den Hartog, T.; Cheng, L.; Wolfs, M.; Habets, R.; Rohlfs, J.; van den Ham, J.; Meulendijks, N.; Sastre, F.; Buskens, P. Using Fiber Bragg Grating Sensors to Quantify Temperature Non-Uniformities in Plasmonic Catalyst Beds under Illumination. *ChemPhotoChem* **2022**. accepted for publication. [[CrossRef](#)]
36. Sharma, S.; Hu, Z.; Zhang, P.; McFarland, E.W.; Metiu, H. CO₂ methanation on Ru-doped ceria. *J. Catal.* **2011**, *278*, 297–309. [[CrossRef](#)]
37. Lach, D.; Zhdan, U.; Smolinski, A.; Polanski, J. Functional and material properties in nanocatalyst design: A data handling and sharing problem. *Int. J. Mol. Sci.* **2021**, *22*, 5176. [[CrossRef](#)]
38. Stöber, W.; Fink, A.; Bohn, E. Controlled Growth of Monodisperse Silica Spheres in the Micron Size Range. *J. Colloid Interface Sci.* **1968**, *26*, 62–69. [[CrossRef](#)]